

Resource-efficient topological fault-tolerant quantum computation with hybrid entanglement of light

S. Omkar,^{*} Y. S. Teo, and H. Jeong[†]

Department of Physics and Astronomy, Seoul National University, 08826 Seoul, Republic of Korea

We propose an all-linear-optical scheme to ballistically generate a cluster state for measurement based topological fault-tolerant quantum computation using hybrid photonic qubits entangled in a continuous-discrete domain. Availability of near-deterministic Bell-state measurements on hybrid-qubits is exploited for the purpose. In the presence of photon-losses, we show that our scheme leads to a significant enhancement in both tolerable photon-loss rate and resource overheads. More specifically, we report a photon-loss threshold of $\sim 3.3 \times 10^{-3}$ which is about an order of magnitude higher than known optical schemes under a reasonable error model. Furthermore, resource overheads to achieve logical error rate of 10^{-6} (10^{-15}) is estimated to be $\sim 6.8 \times 10^5$ (1.4×10^7) which is significantly less by multiple orders of magnitude compared to other known linear optical schemes.

I. INTRODUCTION

Errors during the quantum information processing are unavoidable in a real environment and have been pointed out as a major obstacle against practical implementations of scalable quantum computing [1]. Quantum error correction (QEC) [2] has made it possible to realize scalable quantum computation (QC) with faulty qubits and gates provided the noise is below a certain threshold. The threshold value of the noise is determined by the details of the implementing scheme and the associated noise model.

Measurement-based topological fault-tolerant QC [3] on a *cluster state* is known to provide a high error threshold of 0.75% [4, 5] against the computational errors. Additionally, it can also tolerate qubit-losses [6, 7] and *missing edges* [8], thus a suitable candidate for realizing large scale QC on realistic physical platforms. However, there is a trade-off between the tolerable qubit-losses and missing edges, and the computational error rate, p . A cluster state $|\mathcal{C}\rangle$, over a collection of qubits \mathcal{C} , is the state stabilized by the operators $X_a \otimes_{b \in \text{nh}(a)} Z_b$, where $a, b \in \mathcal{C}$, Z_i and X_i are the Pauli operators on the i th qubit, and $\text{nh}(a)$ represents the adjacent neighborhood of qubit $a \in \mathcal{C}$. It has the form: $|\mathcal{C}\rangle = \prod_{b \in \text{nh}(a)} \text{CZ}_{a,b} |+\rangle_a |+\rangle_b$, $\forall a \in \mathcal{C}$, where CZ is the controlled-Z gate, an entangling operation (EO), and $|\pm\rangle = (|0\rangle \pm |1\rangle)/\sqrt{2}$ are the eigenstates of X , while $|0\rangle, |1\rangle$ are those of Z . Here, we consider the *Raussendorf* cluster state $|\mathcal{C}_{\mathcal{L}}\rangle$ [3] on a cubic lattice \mathcal{L} with qubits mounted on its faces and edges.

The linear optical platform has the advantage of supplying quicker quantum operations on the qubits compared to their decoherence time [9]. Unfortunately, schemes based on discrete variables (DV) like polarizations of light suffer from the drawback that the EO, typically implemented by Bell state measurements, is probabilistic [10]. This leaves the edges corresponding to all failed EOs missing and beyond certain failure rate the cluster state cannot support quantum computation. References [8, 11–13] tackle this shortcoming with a repeat-until-success strategy which incurs extravagant resource over-

heads both in terms of qubits and EO trials, and grows as the success rate of EO falls. Moreover, conditioned on the outcome of the EO all other redundant qubits must be removed *via* measurements [12] which would add to undesirable resource overheads. These schemes also require *active switching*, to select successful outcomes of EO and feed to the next stage, which is known to have adverse effect on photon-loss threshold in optical FTQC [14]. DV based optical EOs have a success rate of 50% that can further be boosted with additional resources like single photons [15], Bell states [16] and the squeezing operation [17]. Ref. [18] uses EOs with boosted success rate of 75% to build cluster states. This can be further enhanced by allotting more resources. Coherent-state qubits enable one to perform nearly deterministic Bell-state measurements and universal QC using linear optics [19, 20], while this approach is generally more vulnerable to losses because it requires photon number parity detectors (PNPDs) [9, 21]. Along this line, a scheme to generate cluster states for topological QC was suggested [22], but the value of α required to build a cluster state of sufficiently high fidelity is unrealistically large as $\alpha > 20$ [22]. A hybrid-qubit using both DV and CV states of light, i.e. polarized single photons and coherent states, was introduced [23], which makes it possible to take advantage of both the approaches to some extent [23].

In this article, we propose an all-linear-optical measurement-based fault-tolerant hybrid topological QC (HTQC) scheme on $|\mathcal{C}_{\mathcal{L}}\rangle$ of hybrid-qubits, which are entangled states of continuous and discrete variables of light. The logical basis for a hybrid-qubit is defined as $\{|\alpha\rangle|H\rangle \equiv |0_L\rangle, |-\alpha\rangle|V\rangle \equiv |1_L\rangle\}$, where $|\pm\alpha\rangle$ are coherent states of amplitudes α , and $|H\rangle$ and $|V\rangle$ are single photon states with horizontal and vertical polarizations in the Z direction. The issues with indeterminism of EOs on DVs and poor fidelity of the cluster states with CVs are overcome by hybrid-qubits. Crucial to our scheme is a near-deterministic hybrid Bell-state measurement (HBSM) on the hybrid-qubits using two PNPDs and two on-off photodetectors (PDs), which is distinct from the previous version that requires two additional PDs to complete a teleportation protocol [23]. In HTQC, we only need HBSMs acting on 3-hybrid-qubit cluster states, which are considered to be offline resource states, to generate $|\mathcal{C}_{\mathcal{L}}\rangle$ without need for active switching

^{*} omkar.shrm@gmail.com

[†] h.jeong37@gmail.com

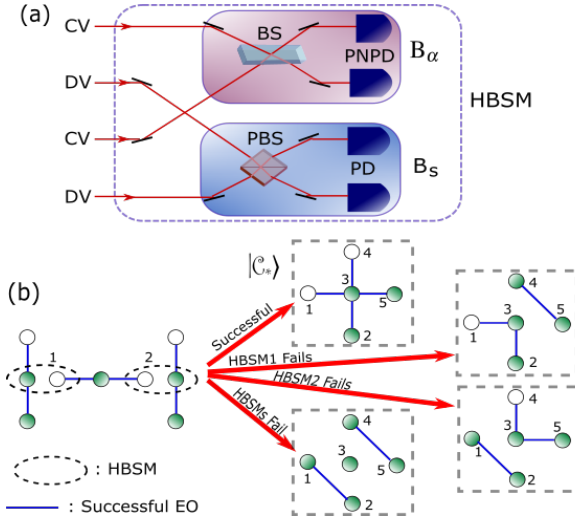


FIG. 1. (Colour online) (a) B_α acts on the CV modes and fails when neither of the two PNPDS click. The failure rate on the hybrid-qubits is $e^{-2\alpha^2}$. B_s acts on the DV modes and is successful with probability 1/2 only when both the PDs click. (b) The 3-hybrid-qubit cluster with an unfilled circle represents $|\mathcal{C}_3\rangle$ while that with two the $|\mathcal{C}_3\rangle$ in Eq. (1). Success of both HBSMs create a star-cluster $|\mathcal{C}_*\rangle$ and other cases leads to cluster states as shown.

and feed-forwarding. In this sense, our scheme is *ballistic* in nature provided the outcomes of HBSMs are noted to interpret the measurement results during the QEC and QC. Both CV and DV modes of a hybrid-qubit support the near-deterministic HBSMs to build the $|\mathcal{C}_\mathcal{L}\rangle$, while only the DV mode suffices for the QEC. This means that only on-off PDs for DV modes are required once a $|\mathcal{C}_\mathcal{L}\rangle$ is generated.

In typical linear optical schemes, apart from the poor success rate of EOs and fidelity, photon-loss is ubiquitous [9] and it causes dephasing of the hybrid-qubits similar to Ref. [21, 23, 24]. We analyze the performance of our scheme against photon losses and compare it with the known linear optical schemes for fault-tolerant QC.

II. PHYSICAL PLATFORM FOR $|\mathcal{C}_\mathcal{L}\rangle$

In order to ballistically build a $|\mathcal{C}_\mathcal{L}\rangle$, we begin with generating the off-line resource states using hybrid-qubits, in the form $(|H\rangle|\alpha\rangle + |V\rangle|-\alpha\rangle)/\sqrt{2} = (|0_L\rangle + |1_L\rangle)/\sqrt{2} \equiv |+_L\rangle$, in addition to passive linear optics elements and PDs. In fact, this type of hybrid qubits with slightly variant forms (with the vacuum and single photon instead of $|H\rangle$ and $|V\rangle$) were generated in recent experiments [25, 26], which can also be used for quantum computing in the same way as [23] even with higher fidelities and success probabilities of teleportation [27]. It is also known that a hybrid qubit can be generated using a Bell-type photon pair, a coherent-state superposition, linear optical elements and four PDs [28].

A HBSM introduced in this letter is composed of two types of measurements, B_α and B_s , acting on the CV and DV modes, respectively. A Bell-state measurement for coherent-

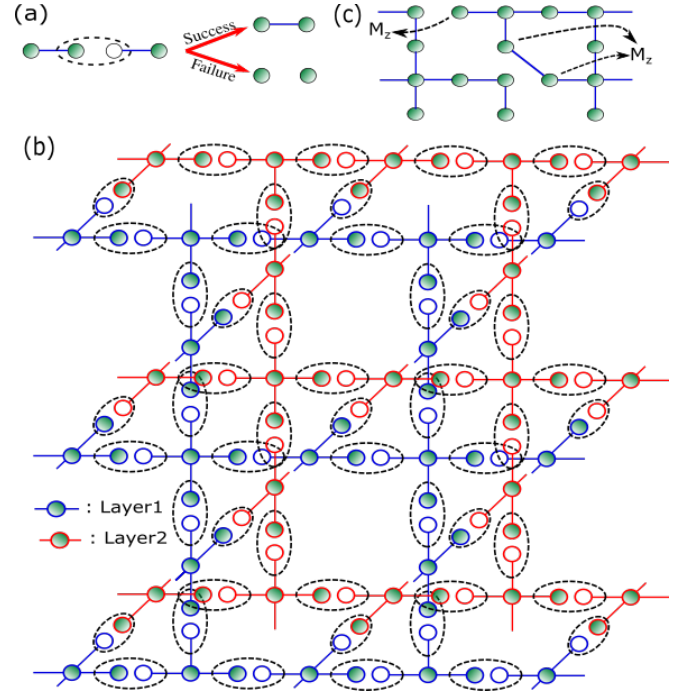


FIG. 2. (Colour online) (a) When connecting $|\mathcal{C}_*\rangle$'s, a successful HBSM creates an edge between hybrid-qubits whereas the failed leaves the edge missing. (b) 3D illustration of building two layers of $|\mathcal{C}_\mathcal{L}\rangle$ for practical HTQC with $|\mathcal{C}_*\rangle$'s and HBSMs to connect them. (c) A diagonal edge is created due to failure of an HBSM corresponding to $|\mathcal{C}_*\rangle$ and a missing edge is due to failure of an HBSM while connecting them. Single layer of $|\mathcal{C}_\mathcal{L}\rangle$ is shown for convenience and M_z is measurement in Z-basis.

state qubits [29], B_α , comprises of a beam splitter (BS) and two PNPDS, whereas B_s has a polarizing beam splitter (PBS) and two PDs as shown in Fig. 1(a). The failure rate for an HBSM turns out to be $p_f = e^{-2\alpha^2}/2$ (deduced in Appendix A, also see Ref. [23]) that rapidly approaches zero with growing α . The first and only nondeterministic step of our protocol is to prepare two kinds of offline-resource states,

$$\begin{aligned}
 |\mathcal{C}_3\rangle &= \frac{1}{2} (|\alpha, \alpha, \alpha\rangle |H, H, H\rangle + |\alpha, \alpha, -\alpha\rangle |H, H, V\rangle \\
 &\quad + |-\alpha, -\alpha, \alpha\rangle |V, V, H\rangle - |-\alpha, -\alpha, -\alpha\rangle |V, V, V\rangle), \\
 |\mathcal{C}_{3'}\rangle &= \frac{1}{\sqrt{2}} (|\alpha, \alpha, \alpha\rangle |H, H, H\rangle + |-\alpha, -\alpha, -\alpha\rangle |V, V, V\rangle)
 \end{aligned} \quad (1)$$

using four hybrid-qubits, two B_α 's and a B_I (type-I fusion gate using two PBSs, two PDs and a $\pi/2$ -rotator as shown in Fig. 6 with a modification to that in Ref. [23]). It has a success probability of 1/2). Construction of $|\mathcal{C}_3\rangle$ and $|\mathcal{C}_{3'}\rangle$ is detailed in Appendix B. Assuming that there is a continuous supply of the offline resource states, the ballistic building of $|\mathcal{C}_\mathcal{L}\rangle$ begins by feeding them into the HBSMs to form *star-clusters* $|\mathcal{C}_*\rangle$ as shown in Fig. 1(b). Simultaneously, they are connected using HBSMs to form layers of $|\mathcal{C}_\mathcal{L}\rangle$ as depicted in Fig. 2(b). As the third dimension of the $|\mathcal{C}_\mathcal{L}\rangle$ is time simulated, in practice only two physical layers suffice for QC [4].

Notably, different outcomes of HBSMs and failures during

this process can be compensated during the QEC as explained below. As HBSMs have four possible outcomes from B_α , the built cluster state will be equivalent to $|\mathcal{C}_L\rangle$ up to local Pauli operations. This can be compensated by accordingly making bit flips to the measurement outcomes during QEC. This is achieved by classical processing and no additional quantum resources are required. As shown in Fig. 1(b), failure of HBSMs results in a cluster states with a diagonal edge instead of four proper edges stretching from the central qubit. Such diagonal edges are inherited by the final cluster as shown in the Fig. 2(c) and disturbs the *stabilizer* structure of $|\mathcal{C}_L\rangle$. However, failure of a HBSM is heralded and reveals the location of such diagonal edge which can be removed by adaptively measuring the hybrid-qubit in Z-basis (M_Z), as shown in Fig. 2(c), restoring back the stabilizer structure. Failure of a HBSM connecting $|\mathcal{C}_*$ s leaves the edge missing as shown in Fig. 2(a) and is part of the resulting cluster as shown in Fig. 2(c) without distorting the stabilizer structure.

III. NOISE MODEL

The predominant errors in optical quantum computing models are due to photon losses [9]. Let η be the photon-loss rate due to imperfect sources and detectors, absorptive optical components and storage. In HTQC, the effect of photon-loss is three fold (see Appendix C and also Ref. [23]): (a) leads to dephasing of hybrid-qubits i.e., phase-flip errors Z , a form of computational error, with rate $p_Z = [1 - (1 - \eta)e^{-2\eta\alpha^2}]/2$, (b) lowers the success rate of HBSM and (c) hybrid-qubits leak out of logical basis. Quantitatively, p_f increases to $(1 - \eta)e^{-2\alpha'^2}/2 + \eta e^{-2\alpha'^2} = (1 + \eta)e^{-2\alpha'^2}/2$, where $\alpha' = \sqrt{1 - \eta}\alpha$. The first term originates from the attenuation of CV mode, and the second from both CV attenuation and DV loss. Thus, for a given η and growing α we face a trade-off between the desirable success rate of HBSM and the detrimental dephasing rate p_Z .

Further, like B_{II} [30], B_s does not introduce computational errors during photon-loss (see Appendix C). However, the action of B_α on the lossy hybrid-qubits introduces additional dephasing as shown in Appendix C 1. To clarify, like DV schemes [13], photon loss do not imply hybrid-qubit loss. In many FTQC schemes η has typical operational value of $\sim 10^{-3}$ (on the higher side) [11, 24, 31, 32], i.e., $\eta \ll 1$. Therefore, the probability of photon-loss leading to hybrid-qubit loss, $\langle 0, 0 | \mathcal{E}(\rho_0) | 0, 0 \rangle = \eta(e^{-\alpha'^2} + e^{-(1+\eta)\alpha'^2})$, where $|0, 0\rangle$ is the two-mode vacuum, is very small compared to p_f and has negligible effect on the HTQC.

IV. MEASUREMENT-BASED HTQC

Once the faulty $|\mathcal{C}_L\rangle$ is built with missing and diagonal edges, and phase-flip errors on the constituent hybrid-qubits, measurement-based HTQC is carried out by making sequential single-qubit measurements in X and Z bases. Few chosen ones are measured in Z -basis to create *defects*, and the

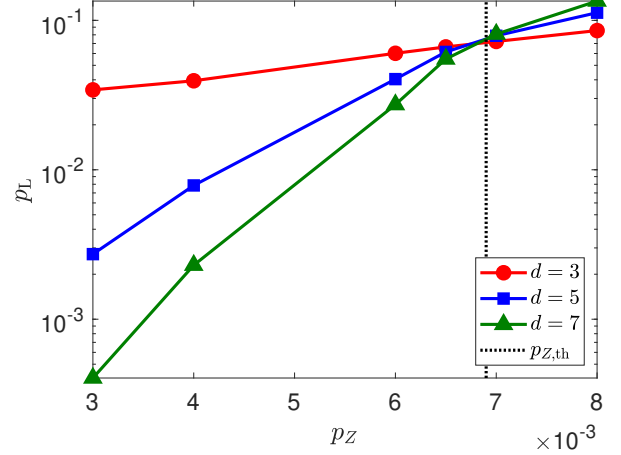


FIG. 3. Logical error rate p_L is plotted against the dephasing rate p_Z for coherent state amplitude $\alpha = 1.247$ and code distances $d = 3, 5, 7$. The intersecting point of these curves correspond to the threshold dephasing rate $p_{Z,th}$.

rest are measured in X -basis for *error syndrome* during QEC and effecting the *Clifford* gates on the logical states of the $|\mathcal{C}_L\rangle$. For *Magic state distillation* measurement is made in the $(X + Y)/\sqrt{2}$ basis [3–5]. All these measurements are accomplished by measuring only the polarization of the DV modes in the respective basis. Note that these measurement outcomes should be interpreted with respect to the recorded HBSM outcomes as mentioned earlier.

V. SIMULATIONS

Simulation of topological QEC is carried out using AUTOTUNE [33]. Only the central hybrid-qubit of $|\mathcal{C}_*\rangle$ remains in the cluster and the rest are utilized by HBSMs. The $|\mathcal{C}_*\rangle$ s are arranged as shown in the Fig. 2. Next, all the hybrid-qubits are subjected to dephasing of rate p_Z following which EOs are performed using HBSMs. The action of B_α in HBSM dephases the adjacent remaining hybrid-qubits which can be modeled as applying $\{Z \otimes I, I \otimes Z\}$ with the rate p_Z . For technical details the readers are referred to Appendix C. This concludes the simulation of building the noisy $|\mathcal{C}_L\rangle$. Further, the hybrid-qubits waiting to undergo measurement as a part of QEC attract dephasing, again the rate p_Z is assigned. During QEC, X -measurement outcomes used for syndrome extraction could be erroneous. This error too is assigned the rate p_Z . Due to photon losses the hybrid-qubits leak out of the logical basis failing the measurement on the DV modes. This leakage too is assigned the rate p_Z which only over estimates the η .

The problem of missing edges due to failed HBSMs can be mapped to two missing hybrid-qubits[8]. Improving on this, by adaptively performing M_Z on one of the hybrid-qubits associated with a missing edge, the missing-edge-problem can be mapped on to a missing qubit [34], see Fig. 2(c). Then, QEC is carried out as in the case of missing qubits [6]. In

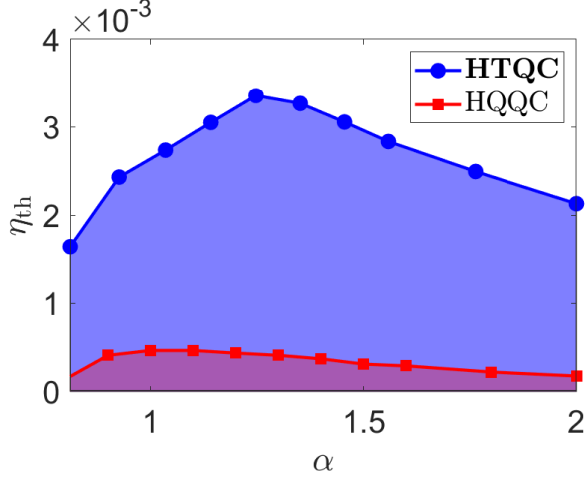


FIG. 4. The tolerable photon loss rate η_{th} is plotted against the coherent state amplitude α . The behavior of the curve is due to trade-off between success rate of HBSM and dephasing rate p_Z with growing α . It can be seen that compared to non-topological HQQC [23], HTQC has an order of higher value for η_{th} .

construction of $|\mathcal{C}_L\rangle$, equal number of HSBMs correspond to building $|\mathcal{C}_*\rangle$ and connecting them, while the former case gives rises to two hybrid-qubit losses and the later to one. Therefore, on an average 1.5 hybrid-qubits are lost. *Percolation threshold* for $|\mathcal{C}_L\rangle$ is 0.249, which is attained by $\alpha = 0.7425$ (when $\eta = 0$), the critical limit below which the HTQC becomes impossible.

VI. RESULTS

The *logical error rate* p_L (rate of failure of topological QEC [4]), was determined against various values of p_Z for $|\mathcal{C}_L\rangle$ of code distances $d = 3, 5, 7$. This was repeated for various values of p_f which correspond to different values of α . Fig. 3 shows the simulation results for $\alpha = 1.247$ in which the intersection point of the curves corresponds to the threshold dephasing rate $p_{Z,th}$. η_{th} is determined using expression for p_Z .

Figure 4 shows the behavior of η_{th} with α . For a given η , owing to trade-off between p_f and p_Z , the optimal value for HTQC is $\alpha_{op} \approx 1.25$ which corresponds to $\eta_{th} \approx 3.3 \times 10^{-3}$ and $p_{Z,th} \approx 6.9 \times 10^{-3}$. The value of η_{th} for $0.8 \leq \alpha \leq 2$ is of the order of 10^{-3} , which is an order greater than the non-topological hybrid-qubit based QC (HQQC) [23] and coherent state QC (CSQC) [21]. HTQC also out performs the topological DV optical scheme with $\eta_{th} \approx 5.5 \times 10^{-4}$ [13]. Multi-photon qubit QC (MQQC) [24], parity state linear optical QC (PLOQC) [31] and error-detecting quantum state transfer based QC (EDQC) [32] provide η_{th} which is lesser than HTQC but of the same order as illustrated in the Fig. 5(a). Note that in Refs. [11, 31, 32], both η and the computational error rates are independent, whereas in our scheme and Refs. [21, 23, 24] these two quantities are related. Also in

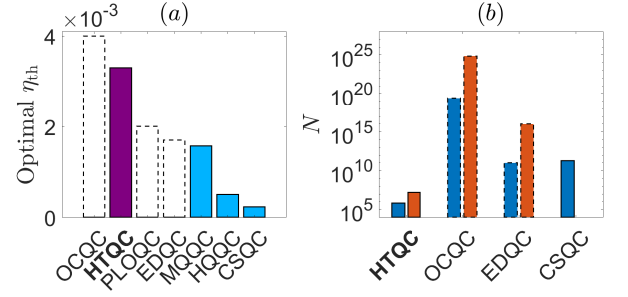


FIG. 5. (a) Illustration of optimal photon-loss threshold η_{th} for various optical QC schemes. It is important to note that the η_{th} 's of OCQC, PLOQC and EDQC (dashed borders) are valid only for zero computational error, which is physically unachievable. All the other schemes evaluate the optimal η_{th} at nonzero computational error that is naturally related to the loss rate η_{th} . (b) Resource overhead N to achieve logical error rate $p_L \sim 10^{-6}$ (blue shorter bars), 10^{-15} (orange taller bars) for known optical schemes. For CSQC we have data only for $p_L \sim 10^{-6}$. Obviously, HTQC is practically favorable for large scale QC both in terms of η_{th} and N .

the former schemes the computational error is dephasing in nature and in the latter schemes it is depolarizing. It is important to note the η_{th} 's claimed by optical cluster-state QC (OCQC) [11], PLOQC and EDQC are valid only for zero computational error rate. This is unrealistic because photon losses typically cause computational errors. For the computational error rate as low as 8×10^{-5} , $\eta_{th} = 0$ for OCQC. Thus, for non-zero computational errors, HTQC outperforms the OCQC too due to its topological nature of QEC.

VII. RESOURCE OVERHEAD

To estimate the resource overhead per gate operation, we count the average number of hybrid-qubits N required to build $|\mathcal{C}_L\rangle$ of sufficiently large side l determined by the target p_L . l is determined such that the $|\mathcal{C}_L\rangle$ can accommodate defects of circumference d which are separated by a distance d [7]. For this, sides must be at least $l = 5d/4$. By extrapolating the suppression of p_L with d , we determine the d required to achieve the target $p_L \approx 10^{-15}$ using Fig. 3. Once the d is determined, N can be estimated as follows. Recall that two $|\mathcal{C}_3\rangle$ s and a $|\mathcal{C}_3\rangle$ are needed to build a $|\mathcal{C}_*\rangle$. On an average, $32/[(4-\eta)(1-e^{-2\alpha^2})^2]$ hybrid-qubits are needed to create a 3-hybrid-qubit cluster (see Appendix C) and a total of $96/[(4-\eta)(1-e^{-2\alpha^2})^2]$ hybrid-qubits for a $|\mathcal{C}_*\rangle$. Each $|\mathcal{C}_*\rangle$ corresponds to a single hybrid-qubit in the $|\mathcal{C}_L\rangle$ and thus the number of $|\mathcal{C}_*\rangle$ needed is $6l^3$. Finally, on an average $1125d^3/[(4-\eta)(1-e^{-2\alpha^2})^2]$ hybrid-qubits are incurred. For $\alpha_{op} \approx 1.25$, $N \approx 6.8 \times 10^5 (1.4 \times 10^7)$ to achieve $p_L \sim 10^{-6} (10^{-15})$. Note that other works consider Bell states [11, 32] and coherent-state qubits [21] as the resource for fault-tolerant QC.

VIII. DISCUSSION

We have proposed an all-linear-optical *ballistic* scheme for measurement-based fault-tolerant topological quantum computation on cluster state built using hybrid-qubits. These exotic entangled states in the continuous-discrete domain simultaneously permit near-perfect cluster states with very few missing edges, and seamless quantum error correction and quantum computation through measurement of the discrete-variable mode. We simulated the performance of our hybrid scheme under the primary source of errors, namely the photon loss that is ubiquitous in any optical system and determined the tolerable photon-loss rate and resource overhead. We compared our results with other optical implementations and found that our scheme is practically favorable than others both in terms of resource overhead and photon-loss threshold (see Fig. 5), especially when exceedingly small logical error rates are desired for large scale quantum computation.

The scheme requires hybrid-qubits of $\alpha \approx \sqrt{2} \times 1.25$ to generate the off-line resource states. In principle, with currently available technology generation of such states is viable

and HTQC is possible by keeping the photon losses below the determined threshold. In this work, we restricted to measurements on the DV modes for QEC. Using the CV modes too, i.e., using more quantum resources, the leakage errors can be overcome and the loss threshold can be further improved.

It is interesting to examine if using other decoders tailored to take advantage of dephasing noise, such as in Ref. [35], can improve the photon-loss threshold. One can also consider different single-qubit noise models [36] and study the performance of the HTQC. As a sideline task, in-situ noise characterization using the available syndrome data [37–40] is feasible. The procedure proposed here to build complex hybrid cluster states can also be used to build lattices of other geometries for QC [18, 41, 42] and in other quantum information endeavors like communication [43].

ACKNOWLEDGMENTS

We thank Dr. Austin G. Fowler for useful discussions and suggestions, and Dr. S.-W. Lee for providing data from Ref. [23] used in Fig. 4 for comparison.

-
- [1] M. A. Nielsen and I. L. Chuang, *Quantum Computation and Quantum Information* (Cambridge University Press, 2010).
 - [2] *Quantum Error Correction* (Cambridge University Press, 2013).
 - [3] R. Raussendorf, J. Harrington, and K. Goyal, *Annals of Physics* **321**, 2242 (2006).
 - [4] R. Raussendorf, J. Harrington, and K. Goyal, *New Journal of Physics* **9**, 199 (2007).
 - [5] R. Raussendorf and J. Harrington, *Phys. Rev. Lett.* **98**, 190504 (2007).
 - [6] S. D. Barrett and T. M. Stace, *Phys. Rev. Lett.* **105**, 200502 (2010).
 - [7] A. C. Whiteside and A. G. Fowler, *Phys. Rev. A* **90**, 052316 (2014).
 - [8] Y. Li, S. D. Barrett, T. M. Stace, and S. C. Benjamin, *Phys. Rev. Lett.* **105**, 250502 (2010).
 - [9] T. C. Ralph and G. J. Pryde, *Progress in Optics*, **54**, 209 (2010).
 - [10] D. E. Browne and T. Rudolph, *Phys. Rev. Lett.* **95**, 010501 (2005).
 - [11] C. M. Dawson, H. L. Haselgrove, and M. A. Nielsen, *Phys. Rev. A* **73**, 052306 (2006).
 - [12] K. Fujii and Y. Tokunaga, *Phys. Rev. Lett.* **105**, 250503 (2010).
 - [13] D. A. Herrera-Martí, A. G. Fowler, D. Jennings, and T. Rudolph, *Phys. Rev. A* **82**, 032332 (2010).
 - [14] Y. Li, P. C. Humphreys, G. J. Mendoza, and S. C. Benjamin, *Phys. Rev. X* **5**, 041007 (2015).
 - [15] F. Ewert and P. van Loock, *Phys. Rev. Lett.* **113**, 140403 (2014).
 - [16] W. P. Grice, *Phys. Rev. A* **84**, 042331 (2011).
 - [17] H. A. Zaidi and P. van Loock, *Phys. Rev. Lett.* **110**, 260501 (2013).
 - [18] M. Gimeno-Segovia, P. Shadbolt, D. E. Browne, and T. Rudolph, *Phys. Rev. Lett.* **115**, 020502 (2015).
 - [19] H. Jeong and M. S. Kim, *Phys. Rev. A* **65**, 042305 (2002).
 - [20] T. C. Ralph, A. Gilchrist, G. J. Milburn, W. J. Munro, and S. Glancy, *Phys. Rev. A* **68**, 042319 (2003).
 - [21] A. P. Lund, T. C. Ralph, and H. L. Haselgrove, *Phys. Rev. Lett.* **100**, 030503 (2008).
 - [22] C. R. Myers and T. C. Ralph, *New Journal of Physics* **13**, 115015 (2011).
 - [23] S.-W. Lee and H. Jeong, *Phys. Rev. A* **87**, 022326 (2013).
 - [24] S.-W. Lee, K. Park, T. C. Ralph, and H. Jeong, *Phys. Rev. Lett.* **114**, 113603 (2015).
 - [25] H. Jeong, A. Zavatta, M. Kang, S.-W. Lee, L. S. Costanzo, S. Grandi, T. C. Ralph, and M. Bellini, *Nature Photonics* **8**, 564 (2014).
 - [26] O. Morin, K. Huang, J. Liu, H. Le Jeannic, C. Fabre, and J. Laurat, *Nature Photonics* **8**, 570 (2014).
 - [27] H. Kim, S.-W. Lee, and H. Jeong, *Quantum Information Processing* **15**, 4729 (2016).
 - [28] H. Kwon and H. Jeong, *Phys. Rev. A* **91**, 012340 (2015).
 - [29] H. Jeong, M. S. Kim, and J. Lee, *Phys. Rev. A* **64**, 052308 (2001).
 - [30] M. Varnava, D. E. Browne, and T. Rudolph, *Phys. Rev. Lett.* **100**, 060502 (2008).
 - [31] A. J. F. Hayes, H. L. Haselgrove, A. Gilchrist, and T. C. Ralph, *Phys. Rev. A* **82**, 022323 (2010).
 - [32] J. Cho, *Phys. Rev. A* **76**, 042311 (2007).
 - [33] A. G. Fowler, A. C. Whiteside, A. L. McInnes, and A. Rabbani, *Phys. Rev. X* **2**, 041003 (2012).
 - [34] J. M. Auger, H. Anwar, M. Gimeno-Segovia, T. M. Stace, and D. E. Browne, *Phys. Rev. A* **97**, 030301 (2018).
 - [35] D. K. Tuckett, S. D. Bartlett, and S. T. Flammia, *Phys. Rev. Lett.* **120**, 050505 (2018).
 - [36] S. Omkar, R. Srikanth, and S. Banerjee, *Quantum Information Processing* **12**, 3725 (2013).
 - [37] S. Omkar, R. Srikanth, and S. Banerjee, *Phys. Rev. A* **91**, 012324 (2015).
 - [38] S. Omkar, R. Srikanth, and S. Banerjee, *Phys. Rev. A* **91**, 052309 (2015).
 - [39] S. Omkar, R. Srikanth, S. Banerjee, and A. Shaji, *Annals of*

Physics **373**, 145 (2016).

- [40] A. G. Fowler, D. Sank, J. Kelly, R. Barends, and J. M. Martinis, arXiv:quant-ph/1405.1454.
 [41] H. Bombin and M. A. Martin-Delgado, Phys. Rev. Lett. **98**, 160502 (2007).
 [42] H. A. Zaidi, C. Dawson, P. van Loock, and T. Rudolph, Phys. Rev. A **91**, 042301 (2015).
 [43] K. Azuma, K. Tamaki, and H.-K. Lo, Nature Communications **6**, 6787 (2015).

Appendix A: Bell State Measurement on hybrid-qubits

The B_α is successful with four possible outcomes that projects the input states of two hybrid-qubits on to one of the four possible hybrid-Bell states:

$$\begin{aligned} |\psi^\pm\rangle &= \frac{1}{\sqrt{2}}(|\alpha, \alpha\rangle |H, H\rangle \pm |-\alpha, -\alpha\rangle |V, V\rangle), \\ |\phi^\pm\rangle &= \frac{1}{\sqrt{2}}(|\alpha, -\alpha\rangle |H, V\rangle \pm |-\alpha, \alpha\rangle |V, H\rangle). \end{aligned} \quad (A1)$$

Action of B_α results as clicks: (even, 0), (odd, 0), (0, even) and (0, odd) on the two photon number parity detectors (PNPD), shown in Fig. 1 (a) of the primary manuscript, when projected on to $|\psi^+\rangle$, $|\psi^-\rangle$, $|\phi^+\rangle$ and $|\phi^-\rangle$, respectively. To see the relation between the clicks on the PNPDs and the hybrid-Bell states, pass the continuous variable (CV) modes through the beam splitter (BS). The states transform as $|\psi^\pm\rangle \rightarrow \frac{1}{\sqrt{2}}(|H, H\rangle + |V, V\rangle)(|\sqrt{2}\alpha\rangle \pm |-\sqrt{2}\alpha\rangle)|0\rangle$, $|\phi^\pm\rangle \rightarrow \frac{1}{\sqrt{2}}(|H, V\rangle + |V, H\rangle)|0\rangle(|\sqrt{2}\alpha\rangle \pm |-\sqrt{2}\alpha\rangle)$. However, there is a possibility of having no clicks on both the PNPDs resulting in failure of the B_α . The probability of failure of B_α on hybrid-qubits is $e^{-2\alpha^2}$.

In spite of failure of the B_α , it is still possible to carry out the Bell measurements using B_{II} on the discrete variable (DV) modes of the hybrid-qubits. The B_{II} makes projection on to the $(|H, H\rangle \pm |V, V\rangle)/\sqrt{2}$ states and is successful with probability 1/2 only when both the photon detectors (PD) click together. The hybrid-Bell state measurement (HBSM) on hybrid-qubits fails only when both B_α and B_{II} fail. Therefore, the probability of failure of HBSM is $\frac{1}{2}e^{-2\alpha^2}$ which rapidly approaches to zero as α grows.

Appendix B: Generation of off-line resource states

Two kinds of three-hybrid-qubit cluster states are used as offline-resources to ballistically generate the *Raussendorf* lattice $|\mathcal{C}\rangle_{\mathcal{L}}$. These two states $|\mathcal{C}\rangle_3$ and $|\mathcal{C}\rangle_{3'}$ differing by Hadamard gate on the extreme qubits are as seen in Eq. 1 of the main manuscript. The reason for need of two kinds of off-line resource state is that for generating the larger cluster states *via* HBSMs, it is required to apply Hadamard gate on one of the two hybrid-qubits taking part [42]; else the resulting states would be only GHZ states. One can also verify this easily. It is important to note that the transformation $|\mathcal{C}\rangle_3 \leftrightarrow |\mathcal{C}\rangle_{3'}$ is not possible via local operations on the hybrid-qubits. So, two types of three-hybrid-qubit clusters have to be generated.

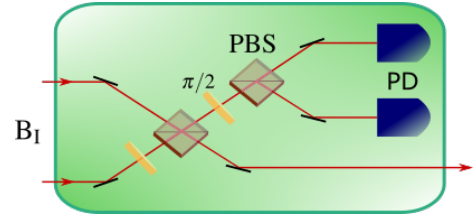


FIG. 6. B_I is an entangling operation, which acts on the DV modes of hybrid-qubits and outputs one mode. It is used to generate the resource states for HTFTQC. B_I is successful with probability 1/2 only when one of the PDs click.

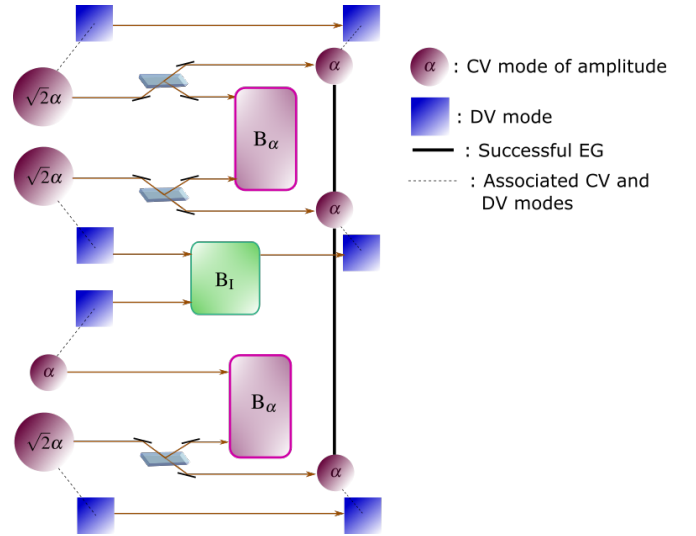


FIG. 7. (Colour online) A schematic diagram to build the offline resource state $|\mathcal{C}\rangle_3$ using two B_α , one B_I and four hybrid-qubits. To create $|\mathcal{C}\rangle_{3'}$, the $\frac{\pi}{2}$ -rotator at the input of B_I is removed.

$|\mathcal{C}\rangle_3$ is generated by entangling three $|+\sqrt{2}\alpha\rangle$ s (hybrid-qubit with CV mode of amplitude $\sqrt{2}\alpha$) and a $|+_L\rangle$ using two B_α s and a B_I . As shown in Fig. 6, B_I has two polarizing BSs (PBS), $\frac{\pi}{2}$ -rotators and two photon detectors (PD). PBS transmits $|V\rangle$ and reflects $|H\rangle$. B_I performs the operation $|H\rangle\langle H| + |H\rangle\langle H, V| + |V\rangle\langle V, H| - |V\rangle\langle V, V|$ which succeeds with probability 1/2 only when one of the PDs click. Instances with no click and both PDs clicking are failures. Hybrid-qubits are initialized as $|+_L^{\sqrt{2}\alpha}\rangle \otimes |+_L^{\sqrt{2}\alpha}\rangle \otimes |+_L\rangle \otimes |+_L^{\sqrt{2}\alpha}\rangle$ and passed on to beam splitters as shown in Fig. 7. The re-

sulting state of the hybrid-qubits is

$$\begin{aligned}
& |\alpha, \alpha, \alpha, \alpha, \alpha, \alpha, \alpha\rangle |H, H, H, H\rangle \\
& + |\alpha, \alpha, \alpha, \alpha, \alpha, -\alpha, -\alpha\rangle |H, H, H, V\rangle \\
& + |\alpha, \alpha, \alpha, \alpha, -\alpha, \alpha, \alpha\rangle |H, H, V, H\rangle \\
& + |\alpha, \alpha, \alpha, \alpha, -\alpha, -\alpha, -\alpha\rangle |H, H, V, V\rangle \\
& + |\alpha, \alpha, -\alpha, -\alpha, \alpha, \alpha, \alpha\rangle |H, V, H, H\rangle \\
& + |\alpha, \alpha, -\alpha, -\alpha, \alpha, -\alpha, -\alpha\rangle |H, V, H, V\rangle \\
& + |\alpha, \alpha, -\alpha, -\alpha, -\alpha, \alpha, \alpha\rangle |H, V, V, H\rangle \\
& + |\alpha, \alpha, -\alpha, -\alpha, -\alpha, -\alpha, -\alpha\rangle |H, V, V, V\rangle \\
& + |-\alpha, -\alpha, \alpha, \alpha, \alpha, \alpha, \alpha\rangle |V, H, H, H\rangle \\
& + |-\alpha, -\alpha, \alpha, \alpha, \alpha, -\alpha, -\alpha\rangle |V, H, H, V\rangle \\
& + |-\alpha, -\alpha, \alpha, \alpha, -\alpha, \alpha, \alpha\rangle |V, H, V, H\rangle \\
& + |-\alpha, -\alpha, \alpha, \alpha, -\alpha, -\alpha, -\alpha\rangle |V, H, V, V\rangle \\
& + |-\alpha, -\alpha, -\alpha, -\alpha, \alpha, \alpha, \alpha\rangle |V, V, H, H\rangle \\
& + |-\alpha, -\alpha, -\alpha, -\alpha, \alpha, -\alpha, -\alpha\rangle |V, V, H, V\rangle \\
& + |-\alpha, -\alpha, -\alpha, -\alpha, -\alpha, \alpha, \alpha\rangle |V, V, V, H\rangle \\
& + |-\alpha, -\alpha, -\alpha, -\alpha, -\alpha, -\alpha, -\alpha\rangle |V, V, V, V\rangle \quad (B1)
\end{aligned}$$

Upon successful $B_\alpha(2,3)$ and $B_\alpha(5,6)$ with respective outcomes, say $|\psi^+\rangle$ and $|\psi^+\rangle$, the state in Eq.(B1) reduces to

$$\begin{aligned}
& |\alpha, \alpha, \alpha\rangle |H, H, H, H\rangle + |\alpha, \alpha, -\alpha\rangle |H, H, V, V\rangle + \\
& |-\alpha, -\alpha, \alpha\rangle |V, V, H, H\rangle + |-\alpha, -\alpha, -\alpha\rangle |V, V, V, V\rangle,
\end{aligned}$$

where $B_\alpha(n,m)$ represents the action of B_α on n -th and m -th CV modes as shown in the Fig. 7. Further, with the successful $B_I(2,3)$ (DV modes 2 and 3 being the inputs as shown in the Fig. 7) we get

$$\begin{aligned}
|\mathcal{C}\rangle_3 = & |\alpha, \alpha, \alpha\rangle |H, H, H\rangle + |\alpha, \alpha, -\alpha\rangle |H, H, V\rangle + \\
& |-\alpha, -\alpha, \alpha\rangle |V, V, H\rangle - |-\alpha, -\alpha, -\alpha\rangle |V, V, V\rangle. \quad (B2)
\end{aligned}$$

Note that for other possible measurement out comes on B_α and B_I the $|\mathcal{C}\rangle_3$ will be equivalent up to local Pauli operations. The local operations to be performed upon getting different measurement comes are listed in Tab. I. The logical Pauli operations on hybrid-qubits can be accomplished with the polarization rotator on the DV mode and the π -phase shifter on the CV mode. X_L : $|\alpha\rangle \leftrightarrow |-\alpha\rangle$, $|H\rangle \leftrightarrow |V\rangle$ and Z_L : $|H\rangle \rightarrow |H\rangle$, $|V\rangle \rightarrow -|V\rangle$ with no need for action on $|\alpha\rangle$. These local operations are used only in creating the offline resource states which is not ballistic process.

Similarly, the $|\mathcal{C}\rangle_{3'}$ can be generated by removing the $\pi/2$ -rotator at the input of the B_I in Fig. 6. Here, the only other possible out come on the B_α s is $|\psi^-\rangle$, in which case the relative phase can be changed by applying a Z_L for the measurement outcome combination $\{|\psi^\pm\rangle, |\psi^\mp\rangle\}$. $|\mathcal{C}\rangle_3$ and $|\mathcal{C}\rangle_{3'}$ are created only when the two B_α and B_I succeed together. The probability that all the three operations are successful is $\frac{1}{2}(1 - e^{-2\alpha^2})^2$. Thus, the average number of hybrid-qubits consumed for generating a $|\mathcal{C}\rangle_3$ or $|\mathcal{C}\rangle_{3'}$ is $8/(1 - e^{-2\alpha^2})^2$.

$B_\alpha(2,3)$	$B_\alpha(5,6)$	$B_I(2,3)$	Local Operation
$ \psi^+\rangle$	$ \psi^+\rangle$	H/V	NA/ Z_3
$ \psi^+\rangle$	$ \psi^-\rangle$		Z_3/Z_2Z_3
$ \psi^+\rangle$	$ \phi^+\rangle$		Z_2/NA
$ \psi^+\rangle$	$ \phi^-\rangle$		$Z_2Z_3/X_3Z_2Z_3$
$ \psi^-\rangle$	$ \psi^+\rangle$	H/V	Z_2/NA
$ \psi^-\rangle$	$ \psi^-\rangle$		Z_2Z_3/Z_3
$ \psi^-\rangle$	$ \phi^+\rangle$		NA/ Z_2
$ \psi^-\rangle$	$ \phi^-\rangle$		$X_3Z_2Z_3/Z_2Z_3$
$ \phi^+\rangle$	$ \psi^+\rangle$	H/V	X_1/X_1Z_1
$ \phi^+\rangle$	$ \psi^-\rangle$		$X_2/X_1Z_2Z_3$
$ \phi^+\rangle$	$ \phi^+\rangle$		X_1Z_2/X_1
$ \phi^+\rangle$	$ \phi^-\rangle$		$X_1Z_2Z_3/X_1Z_3$
$ \phi^-\rangle$	$ \psi^+\rangle$	H/V	$X_2Z_2Z_3/X_1$
$ \phi^-\rangle$	$ \psi^-\rangle$		X_2Z_2/X_2
$ \phi^-\rangle$	$ \phi^+\rangle$		X_1/X_1Z_2
$ \phi^-\rangle$	$ \phi^-\rangle$		$X_2/X_1Z_2Z_3$

TABLE I. The table lists the local operations to be performed upon getting different measurement comes on B_α and B_I

Appendix C: Hybrid-qubits under photon-loss

The action of the photon-loss channel \mathcal{E} on a hybrid-qubit initialized in the state $\rho_0 = |+_L\rangle\langle+_L|$ is [23]

$$\begin{aligned}
\mathcal{E}(\rho_0) = & (1 - \eta) \left(\frac{1 + e^{-2\eta\alpha^2}}{2} |+\rangle\langle+| + \right. \\
& \left. + \frac{1 - e^{-2\eta\alpha^2}}{2} |-\rangle\langle-| \right) + \frac{\eta}{2} \left(|+\rangle\langle+| + |-\rangle\langle-| \right) \\
= & \frac{(1 - \eta)}{2} \left(|\alpha', H\rangle\langle\alpha', H| + |-\alpha', V\rangle\langle-\alpha', V| \right. \\
& \left. + e^{-2\eta\alpha^2} (|\alpha', H\rangle\langle-\alpha', V| + |-\alpha', V\rangle\langle\alpha', H|) \right) \\
& + \frac{\eta}{2} \left((|\alpha'\rangle\langle\alpha'| + |-\alpha'\rangle\langle-\alpha'|) \otimes |0\rangle\langle 0|, \right. \\
& \left. + e^{-2\eta\alpha^2} (|\alpha'\rangle\langle-\alpha'| + |-\alpha'\rangle\langle\alpha'|) \otimes |0\rangle\langle 0| \right) \quad (C1)
\end{aligned}$$

where $|\pm'\rangle = (|\alpha', H\rangle \pm |-\alpha', V\rangle)/\sqrt{2}$, $|\pm^k\rangle = (|\alpha'\rangle \pm |-\alpha'\rangle) \otimes |0\rangle/\sqrt{2}$ and $\alpha' = \sqrt{1 - \eta}\alpha$ with η being photon loss rate which also models imperfect sources, detectors, or absorptive optical components. It can be seen from the Eq. (C1), that due to photon-loss the CV part is dephased and the loss on the DV part make the hybrid-qubits leak out of the logical basis. Also, due to photon-losses the success rate of the B_α reduces to $(1 - e^{-2\alpha^2})$ and that of B_I to $(1/2 - \eta/8)$. As a result, the average number of hybrid-qubits to build off-line resource states increases to $32/[(4 - \eta)(1 - e^{-2\alpha^2})^2]$.

Loss-tolerance of B_I : One can verify that the noisy DV part in Eq. B2, $\mathcal{E}^{\otimes 4}(|H, H, H, H\rangle + |H, H, V, V\rangle + |V, V, H, H\rangle + |V, V, V, V\rangle)$ is transformed in to $\mathcal{E}^{\otimes 3}(|H, H, H\rangle + |H, H, V\rangle +$

$|v, v, H\rangle - |v, v, v\rangle$) under the action of B_I . The noise channel on the resulting state is still \mathcal{E} , implying that no additional computational errors are introduced by B_I , unlike in Ref. [14].

1. Noise by HBSM under photo-loss



FIG. 8. (Colour online) Typical instance of action of HBSM on the noisy hybrid-cluster states.

Let us consider the typical situation where HBSMs are used to create entanglement between the desired hybrid-qubits as shown in the Fig. 8. Looking at only the CV part, we have

$$(|\alpha, \alpha\rangle + |\alpha, -\alpha\rangle + |-\alpha, \alpha\rangle - |-\alpha, -\alpha\rangle)(|\alpha, \alpha\rangle + |-\alpha, -\alpha\rangle). \quad (C2)$$

To determine the noise on the resultant cluster state after the action of B_α , we consider the hybrid-qubits undergoing BSM to be noisy. The resulting noisy state, in the logical basis is of the form

$$\frac{1}{4} \begin{pmatrix} 1 & e^{-4\eta\alpha^2} & 1 & e^{-4\eta\alpha^2} \\ e^{-4\eta\alpha^2} & 1 & e^{-4\eta\alpha^2} & 1 \\ 1 & e^{-4\eta\alpha^2} & 1 & e^{-4\eta\alpha^2} \\ e^{-4\eta\alpha^2} & 1 & e^{-4\eta\alpha^2} & 1 \end{pmatrix}. \quad (C3)$$

For the desired result of the HBSMs, the Hadamard could be on the other hybrid-qubit too where the terms in the Eq. C2 are interchanged and the resulting noisy state is

$$\frac{1}{4} \begin{pmatrix} 1 & 1 & e^{-4\eta\alpha^2} & e^{-4\eta\alpha^2} \\ 1 & 1 & e^{-4\eta\alpha^2} & e^{-4\eta\alpha^2} \\ e^{-4\eta\alpha^2} & e^{-4\eta\alpha^2} & 1 & 1 \\ e^{-4\eta\alpha^2} & e^{-4\eta\alpha^2} & 1 & 1 \end{pmatrix}. \quad (C4)$$

Considering both the instances of action of B_α , the resultant state is the equal weighted superposition of the states in Eq. (C3) and Eq. (C4), and the corresponding Kraus operators for this noisy channel \mathcal{E}^{B_α} are $\left\{ \sqrt{\frac{1+e^{-4\eta\alpha^2}}{2}} I \otimes I, \sqrt{\frac{1-e^{-4\eta\alpha^2}}{4}} Z \otimes I, \sqrt{\frac{1-e^{-4\eta\alpha^2}}{4}} I \otimes Z \right\}$. This noise channel \mathcal{E}^{B_α} is used as the noise due to entangling operation in the AUTOTUNE [33]. We observe that for $\eta \sim 10^{-3}$ and small values of α , $p_Z \approx (1 - e^{-4\eta\alpha^2})/4$. Thus, the \mathcal{E}^{B_α} will have the following Kraus operators $\left\{ \sqrt{(1+p_Z)/2} I \otimes I, \sqrt{\eta\alpha^2} Z \otimes I, \sqrt{p_Z} I \otimes Z \right\}$.

Loss-tolerance of B_s : Now, let's move our attention towards the DV part of the noisy cluster states as shown in the Fig. 8 and study the action of B_s on them during photon loss. One can verify that the state $\mathcal{E}(|H, H\rangle + |v, v\rangle) \otimes (|H, H\rangle + |H, v\rangle + |v, H\rangle - |v, v\rangle)$ is transformed to $\mathcal{E}(|H, H\rangle + |H, v\rangle + |v, H\rangle - |v, v\rangle)$ under the action of B_s . The noise channel on the resulting state is still \mathcal{E} which confirms that the B_s introduces no additional computational errors.